THE JOURNAL OF BIOLOGICAL CHEMISTRY VOL. 290, NO. 27, pp. 16744–16758, July 3, 2015

The Wnt Inhibitor Sclerostin Is Up-regulated by Mechanical Unloading in Osteocytes *in Vitro*[*]

Received for publication, December 11, 2014, and in revised form, May 5, 2015 Published, JBC Papers in Press, May 7, 2015, DOI 10.1074/jbc.M114.628313

Jordan M. Spatz[‡§1], Marc N. Wein[‡], Jonathan H. Gooi[¶], Yili Qu[‡], Jenna L. Garr[‡], Shawn Liu[‡], Kevin J. Barry[‡], Yuhei Uda[‡], Forest Lai[‡], Christopher Dedic[‡], Mercedes Balcells-Camps[§‖2], Henry M. Kronenberg[‡], Philip Babij[**], and Paola Divieti Pajevic[‡3]

From the [‡]Endocrine Unit, Massachusetts General Hospital and Harvard Medical School, Boston, Massachusetts 02114, [§]Harvard-MIT Institute for Medical Engineering and Science, Massachusetts Institute of Technology, Cambridge, Massachusetts 02139, [‖]Bioengineering Department, Institut Quimic de Sarria, Ramon Llull University, 08017 Barcelona, Spain, [¶]NorthWest Academic Centre, The University of Melbourne, St. Albans, Victoria 3065, Australia, and [**]Amgen Inc., Thousand Oaks, California 91320

Background: Recent studies have suggested osteocytes as key players in mechanosensation and skeletal metabolism.
Results: Simulated microgravity induces an autonomous up-regulation of *SOST*/sclerostin and *RANKL*/*OPG* in a novel osteocytic cell line, Ocy454.
Conclusion: Mechanical loading regulates intrinsic osteocyte responses in concert with hormonal and cytokine inputs.
Significance: Learning how osteocytes sense mechanical loads would enable novel interventions to prevent disuse-induced bone loss.

Although bone responds to its mechanical environment, the cellular and molecular mechanisms underlying the response of the skeleton to mechanical unloading are not completely understood. Osteocytes are the most abundant but least understood cells in bones and are thought to be responsible for sensing stresses and strains in bone. Sclerostin, a product of the *SOST* gene, is produced postnatally primarily by osteocytes and is a negative regulator of bone formation. Recent studies show that *SOST* is mechanically regulated at both the mRNA and protein levels. During prolonged bed rest and immobilization, circulating sclerostin increases both in humans and in animal models, and its increase is associated with a decrease in parathyroid hormone. To investigate whether *SOST*/sclerostin up-regulation in mechanical unloading is a cell-autonomous response or a hormonal response to decreased parathyroid hormone levels, we subjected osteocytes to an *in vitro* unloading environment achieved by the NASA rotating wall vessel system. To perform these studies, we generated a novel osteocytic cell line (Ocy454) that produces high levels of *SOST*/sclerostin at early time points and in the absence of differentiation factors. Importantly, these osteocytes recapitulated the *in vivo* response to mechanical unloading with increased expression of *SOST* (3.4 ± 1.9-fold, $p < 0.001$), sclerostin (4.7 ± 0.1-fold, $p < 0.001$), and the receptor activator of nuclear factor κB ligand (*RANKL*)/osteoprotegerin (*OPG*) (2.5 ± 0.7-fold, $p < 0.001$) ratio. These data demonstrate for the first time a cell-autonomous increase in *SOST*/sclerostin and *RANKL*/*OPG* ratio in the setting of unloading. Thus, targeted osteocyte therapies could hold promise as novel osteoporosis and disuse-induced bone loss treatments by directly modulating the mechanosensing cells in bone.

It has been recognized for over a century that mechanical loading is fundamental for the normal development and maintenance of the musculoskeletal system. Reduced loading is prevalent in our aging population, in the setting of spinal cord and other injuries, in prolonged bed rest, as a result of significant weight loss, or as experienced by astronauts during space flight and is invariably associated with bone loss (1–7). Although it has been appreciated for more than a century that bone models itself in response to its mechanical environment (Wolff's law) (8), the mechanisms underlying this response still need to be fully elucidated. Osteocytes are the most abundant but least understood bone cell type. Because osteocytes exhibit a dendritic morphology with extensive connectivity throughout the mineralized matrix of bone, it is thought that this system forms the bone mechanosensor, acting as the orchestrator of osteoblast and osteoclast activity in response to mechanical stimuli (9–11). Osteocyte ablation results in a resistance to disuse-induced bone loss, highlighting the central role osteocytes play as the mechanosensor of bone (12). Improved understanding of the molecular mechanisms of osteocyte mechanosensation could have significant implications for the treatment of bone disorders including osteoporosis, fracture healing, and disuse-induced bone loss.

The precise mechanisms whereby osteocytes respond to and convert mechanical stimuli to biochemical signals remain elusive because of a lack of appropriate *in vitro* models. At the molecular level, osteocytes are thought to regulate the response

[*] This work was supported, in whole or in part, by National Institutes of Health Grants AR059655 from the NIAMS (to P. D. P.) and DK011794 (to H. M. K.) and DK100215 (to M. N. W.) from the NIDDK. P. Babij was employed by Amgen Inc. and received Amgen stock.
[1] Supported by a Northrop Grumman Aerospace Systems Ph.D. training fellowship, a Massachusetts Institute of Technology Hugh Hampton Young fellowship, the National Space Biomedical Research Institute through NASA Grant NCC 9-58, and the United States Army Institute for Environmental Medicine Oak Ridge Science Institute for Science and Education fellowship program.
[2] Supported by Spain's Ministerio de Economia e Innovacion (Grant SAF2013-43302-R), Posimat, and Fundacio Empreses Institut Químic de Sarrià.
[3] To whom correspondence should be addressed: Molecular and Cell Biology, Goldman School of Dental Medicine, Boston University, 700 Albany St., Boston, MA 02118. E-mail: pdivieti@bu.edu.

of bone to mechanical loading by at least two key molecules, sclerostin and receptor activator of nuclear factor κB ligand (*RANKL*)[4] (9, 13). Mature osteocytes are one of the few cells that postnatally produce sclerostin, which is encoded by the *SOST* gene. Sclerostin inhibits bone formation both *in vitro* and *in vivo* by directly reducing proliferation and differentiation of osteoblasts via the canonical Wnt signaling pathway. Sclerostin is thought to act by binding low density lipoprotein receptors 5 and 6 to inhibit Wnt-β-catenin signaling (14–16). Moreover, sclerostin appears central to the response of bone to mechanical loading. *SOST*/sclerostin expression increases with mechanical unloading (10, 17) and decreases with loading (10). In addition, *SOST* knock-out mice are resistant to disuse-induced bone loss (18), and mice treated with sclerostin antibody show an anabolic response in the hind limb unloaded model (19). Furthermore, serum sclerostin is significantly increased during prolonged (90-day) bed rest in healthy volunteers (17), in obese patients undergoing weight loss (20), and acutely in postmenopausal stroke patients (21). In addition to the effects of sclerostin, it was recently shown that soluble *RANKL* also secreted by osteocytes (9, 13) contributes to the control of bone remodeling. However, *RANKL* has also been found to be expressed in a variety of other cell types including osteoblasts, bone lining cells, keratinocytes, T and B lymphocytes, mammary epithelial cells, and undefined cell types within the brain (22). Thus, it is currently unknown whether osteocytes can increase *RANKL* in a cell-autonomous manner, thus potentially serving as an initiator of the cascade of bone resorption seen in mechanical unloading and microgravity.

Regardless of the initiation mechanisms, the hallmark of immobilization and microgravity in humans is an increase in bone resorption (23, 24), resulting in subsequent transient hypercalcemia with persistently increased urinary and fecal calcium loss (23). The endocrine counter-regulatory mechanisms to maintain normal serum calcium are a reduction in serum parathyroid hormone (PTH) and consequently lower 1,25-dihydroxyvitamin D concentrations (23). However, PTH is also a known potent regulator of *SOST*/sclerostin in osteocytes both in humans and in animal models (25, 26), raising the possibility that the increase in *SOST*/sclerostin during unloading or bed rest might be a consequence of decreased serum PTH rather than direct mechanical sensing by osteocytes. Indeed, there is an inverse correlation between PTH and sclerostin in male hypoparathyroid subjects (27), and PTH infusion in healthy men induces a decline in circulating sclerostin (28). Both *in vivo* and *in vitro*, PTH decreases sclerostin expression via activation of the PTH receptor expressed on osteocytes (29), and mice lacking the PTH receptor specifically in osteocytes have elevated expression of sclerostin (30). Thus, *in vivo* studies cannot determine whether suppression of PTH or other changes in cytokines, such as prostaglandin E_2 (PGE_2), are driving the increases in serum sclerostin following unloading. More broadly, there is no evidence to assess whether the increase in *SOST*/sclerostin is a direct osteocyte response to mechanical unloading as postulated by the mechanostat theory proposed by Harold Frost (31).

Currently available osteocytic cell lines express basally very low levels of *SOST*/sclerostin and require high cell density with extended time in culture under differentiation conditions to produce detectable *SOST*/sclerostin (32–34), thus limiting their use for investigating mechanotransduction signaling pathways. To investigate osteocyte responses to unloading, we have isolated and characterized a novel osteocytic cell line (Ocy454), reported herein, that faithfully recapitulates the *in vivo* response of osteocytes to mechanical stimuli. Ocy454 cells show rapid, high level expression of *SOST*/sclerostin that is responsive to hormonal (PTH), cytokine (PGE_2), and mechanical stimuli. Furthermore, $G_s\alpha$ knockdown in Ocy454 led to significant increases in *SOST* expression matching known osteocyte *in vivo* regulation (35), demonstrating the broad utility of this new osteocytic cell line for studying *SOST*/sclerostin regulation as we have recently reported (36). Ocy454 also showed an enhanced osteocytic phenotype when cultured on a three-dimensional biomaterial by increasing *FGF23* expression upon PTH stimulation, highlighting the importance of optimizing *in vitro* culture conditions for studying certain aspects of osteocyte biology.

The primary hypothesis and objective of this study were to determine whether mechanical unloading is sensed in an osteocyte-endogenous manner and investigate the cellular mechanism(s) osteocytes utilize to regulate *SOST*/sclerostin. We hypothesized that simulated unloading (microgravity) as achieved in the NASA rotating wall bioreactors would increase *SOST*/sclerostin in a cell-autonomous fashion and that this increase would be suppressible by negative regulators (PTH and PGE_2) of *SOST*/sclerostin. As reported herein, osteocytic cells are indeed capable of responding to reduced mechanical forces with time-dependent increases in *SOST*/sclerostin expression. In addition, the gene expression profile in simulated microgravity (*e.g. SOST*, osteocalcin, *Phex*, and *MEPE*) is distinct from that seen with mechanical loading as achieved by fluid shear stress. Moreover, the increase in *SOST*/sclerostin expression is suppressed by PTH and PGE_2, suggesting upstream mechanistic overlap between mechanical sensing and G-protein-coupled receptor signaling and the potential to use targeted therapies in these signaling pathways as treatments for disuse-induced bone loss.

Experimental Procedures

Osteocytic Cell Lines—Mice expressing the green fluorescent protein (*GFP*) under the control of dentin matrix protein 1 (8-kb *DMP1-GFP*) (kindly provided by Dr. Ivo Kalajzic, University of Connecticut Health Center) (37) were mated with mice carrying a ubiquitously expressed SV40 large T antigen (Immortomouse, Charles River), and osteocytes were isolated from the long bones of 4-week-old double transgenic mice. Long bones were cut at the epiphysis; flushed with medium (α-minimum Eagle's medium) (Gibco) supplemented with 0.1% bovine serum albumin, 25 mM HEPES (pH 7.4) and containing 1 mg/ml collagenase type I:II (ratio, 1:3) (Worthington); and subjected to four sequential collagenase digestions, one EDTA digestion, and a final sixth collagenase digestion, and

[4] The abbreviations used are: RANKL, receptor activator of nuclear factor κB ligand; PTH, parathyroid hormone; OPG, *osteoprotegerin; PGE_2,* prostaglandin E_2; *DMP1,* dentin matrix protein 1; hPTH, human PTH.

minced bone fragments were placed in collagen-coated 100-mm tissue discs. Cells were allowed to reach confluence at 33 °C and then grown for an additional 10–12 days at 37 °C prior to FACS for *DMP1-GFP* expression. Bulk-sorted *GFP*-positive cells were maintained on collagen-coated flasks grown in α-minimum Eagle's medium supplemented with 10% FBS (Gibco) and 1% antibiotic-antimycotic (Gibco). Subsequently, two criteria were selected for further identification of a mature osteocytic cell line: sorted *GFP*-positive were required to 1) have high levels of production of known osteocytic genes (*SOST* and *DMP1*) at the early time point of 14 days at the semipermissive temperature in the absence of differentiation and 2) respond to the known effects of PTH stimulation by suppression of *SOST* and increased expression of *RANKL*. This method provided a heterogeneous population of *DMP1-GFP*-positive cells that more faithfully resemble osteocytes *in vivo*, which are known to be a mixture of cells with various degrees of *SOST* and *DMP1* expression depending on their age/maturation. We performed our experiments in this heterogeneous population. In an effort to establish a more homogeneous osteocytic population, we also performed FACS on Ocy454 to isolate single cell subclones. Ocy454 and several single cell clones (36) have the same osteocyte marker expression and hormonal (PTH, PGE_2, and shear stress) response.

For two-dimensional cell culture, cells (Ocy454, IDG-SW3 (33), and primary long bone osteoblasts isolated from 4-week-old SV40 large T antigen mice) were plated at 10^5 cells/ml and allowed to reach confluence at the permissive temperature (33 °C) for 3 days. Subsequently, cells were either differentiated at the permissive temperature or switched to the semipermissive temperature (37 °C) for the indicated time points. MLO-Y4 cells were plated at 10^5 cells/ml, and RNA was extracted at 4 days (32). For primary osteocytes, cells were isolated from 4-week-old *DMP1-GFP* long bones. In brief, long bones were flushed of bone marrow with PBS, subjected to sequential collagenase digestions, and minced, and bone chips were placed in tissue culture plates. Subsequently, at the 2-week time point, cells were subjected to FACS. *GFP*− and *GFP*+ populations were directly collected into RNA extraction buffer (Qiagen).

The routine culturing conditions to maintain the Ocy454 osteocytic phenotype were twice weekly subpassages (1:5) for up to 4 months from a frozen stock. For three-dimensional cell culture, 1.6×10^6 Ocy454 cells were plated on 200-μm polystyrene Alvetex (Reinnervate) well insert scaffolds. Scaffolds were collagen-coated according to the manufacturer's protocols for the indicated experiments. All other chemicals were from Sigma-Aldrich or Fisher Scientific.

Quantitative Real Time PCR—Total RNA was isolated (RNAEasy, Qiagen, Valencia, CA) according to the manufacturer's recommendations, and RNA was quantified (NanoDrop, Thermo Scientific, Rockford, IL). cDNA synthesis was performed (Qiagen or Taraka Clontech) on 0.5–1 μg of total RNA followed by SYBR quantitative PCR (StepOnePlus, Life Technologies). Primer sequences are available upon request. β-Actin (*ACTB*) or *HPRT1* was used for normalization of gene expression. ΔCT was computed within each sample to the housekeeping reference, and ΔΔCT was computed across experimental conditions. Experiments were run in triplicates unless otherwise indicated.

Western Blot—Whole cell lysates (Mammalian Protein Extraction Reagent, Thermo Scientific) from two-dimensional cell culture conditions were prepared according to the manufacturer's recommendations. Protein concentrations were quantified (Bio-Rad Protein Assay, Bio-Rad), and 10 μg was separated on a 4–20% Tris-glycine denaturing gel (Life Technologies) and transferred to a PVDF membrane using the Trans-Blot Turbo (Bio-Rad) system according to the manufacturer's recommendations. The membrane was blocked with 3% BSA and 5% nonfat milk in Tris-buffered saline containing 0.05% Tween 20 (TBST) for 1 h and then incubated with goat polyclonal mouse sclerostin antibody (1:200; R&D Systems, Minneapolis, MN) overnight at 4 °C (30). After washing, secondary antibody (1:5000) was incubated for 1 h at room temperature and then developed using enhanced chemiluminescence (Thermo Scientific) (30). For $G_s\alpha$ immunoblotting, similar procedures were followed using an anti-$G_s\alpha$ antibody (Millipore, catalogue number 06-237).

Sclerostin Immunohistochemistry—Three-dimensional scaffolds were washed once with phosphate-buffered saline (Life Technologies) and frozen embedded (OCT, Tissue Tek), and 10-μm sections were cut onto standard microscope slides. In brief, proteinase K was used for antigen retrieval for 15 min followed by a quench in 3% H_2O_2, methanol for 10 min, washing in H_2O, and rinsing in 1× TBS. Next, biotinylated anti-sclerostin antibody (R&D Systems, BAF1589) diluted 1:50 in Tris-NaCl blocking buffer was incubated for 1 h and washed three times with 1× Tris-NaCl-Tween buffer. Streptavidin-HRP diluted 1:100 in Tris-NaCl blocking buffer was then added to slides and incubated for 30 min, washed three times with 1× Tris-NaCl-Tween buffer, and incubated with 3,3′-diaminobenzidine HRP substrate (Vector Labs) for 5 min, and the slide was coverslipped.

Sclerostin ELISA—Four milliliters of cell culture supernatants from slow turning rotating wall bioreactor experiments at the indicated time points were spun at 850 rpm for 4 min, and the volume was reduced to 250 ml with a 10-kDa centrifugal filter unit (Millipore, Billerica, MA) according to the manufacturer's recommendations. Supernatants were assayed for sclerostin using a commercially available assay (ALPCO, Salem, NH) according to the manufacturer's recommendations. For additional sclerostin ELISA experiments, an antibody matched pair ELISA was used (34). In brief, for the matched pair sclerostin ELISA, conditioned medium (36–48 h) was harvested from Ocy454 cells as indicated in the figure legends and stored at −80 °C until further use. High binding 96-well plates (Fisher, 21-377-203) were coated with sclerostin antibody VI capture antibody (3 μg/ml) in PBS for 1 h at room temperature. Plates were washed (PBS plus 0.5% Tween 20) and blocked with wash buffer supplemented with 1% BSA and 1% normal goat serum for 1 h at room temperature. Samples (60 μl/well) were then added along with a standard curve of murine recombinant sclerostin (ALPCO), and plates were incubated overnight at 4 °C. Plates were washed three times and incubated with HRP-coupled sclerostin antibody VII detection antibody (0.5 μg/ml) for 1 h at room temperature. After washing, signal detection

TABLE 1
shRNA target sequences

shRNA	Target sequences
LacZ	CCAACGTGACCTATCCCATTA
Luciferase	AGAATCGTCGTATGCAGTGAA
GNAS E3	CGCAGATAAGAAACGCAGCAA
GNAS B2	GCCAAGTACTTCATTCGGGAT
GNAS G2	TCGGGATGAGTTTCTGAGAAT
GNAS G9	CCTGCATGTTAATGGGTTTAA
GNAS C2	CCTGAAGAATCTGTGCCATTT

was performed using Ultra 3,3′,5,5′-tetramethylbenzidine ELISA (Pierce, 34028), stopped by 2 N sulfuric acid, and read at 450 nm. Prior to harvesting supernatant, cell number per well was always determined using the PrestoBlue assay (Life Technologies) according to the manufacturer's instructions.

For shRNA experiments, shRNA (Broad Institute, Cambridge, MA) lentiviral particles in puromycin-resistant vector targeted against luciferase (control; shLuciferase) or sh$G_s\alpha$ were used to infect cells plated 1 day prior at 0.5×10^5 cells/ml. Subsequently, infected cells were puromycin-selected (2 μg/ml) at the permissive temperature (33 °C) for 7 days and subsequently allowed to differentiate for 14–16 days at the semipermissive temperature. Table 1 provides the shRNA target sequences.

Simulated Microgravity—Ocy454 cells were plated on three-dimensional scaffolds as described above and allowed to grow at the permissive temperature (33 °C) for 3 days. Subsequently, scaffolds were moved to the semipermissive temperature (37 °C) for an additional culturing time before being loaded into the bioreactor. Scaffolds were cut into 3-mm discs using disposable biopsy punches (Integra Miltex, Plainsboro, NJ) and placed into non-rotating (static) or rotating (simulated microgravity) 110-ml slow turning lateral vessels (Synthecon, Houston, TX) for 3 days. For the rotating vessels, rotation speed was set to 18.6 rpm for the first 24 h and increased to 20.9 rpm to maintain solid body rotation kinetics throughout the experiment (38).

Two-dimensional Laminar Fluid Shear Stress—Ocy454 cells were plated on glass microscope culture slides (Flexcell International Corp.) at 2×10^5 cells/ml and allowed to grow at the permissive temperature (33 °C) for 3 days. Subsequently, slides were moved to the semipermissive temperature (37 °C) for an additional culturing time (11–14 days). Medium was changed for static slides, or slides were loaded into the laminar fluid flow shear stress device (Flexcell Streamer, Flexcell International Corp.) connected to an electronically controlled peristaltic pump with pulse dampers integrated into the flow circuit to allow for continuous unidirectional shear stress. Cells were exposed to 0.5 or 2 dynes/cm^2 for 2 h or 3 days (39–41).

Three-dimensional Fluid Shear Stress—Alvetex scaffolds were seeded with 1.6 10^6 cells and allowed to grow at the permissive temperature (33 °C) for 2 days prior to transferring to (37 °C) for differentiation. Cells were differentiated for 14 days prior to transferring to the Reinnervate perfusion plate. The perfusion plates were attached to a Masterflex peristaltic pump (catalog number 7520-57) with a Masterflex standard pump head (catalog number 7014-20) and exposed to either 0.5 or 2 dynes/cm^2 for either 1 or 3 days.

Statistical Analysis—All values are reported as the mean ± S.D. unless otherwise noted. Group mean differences were evaluated with Student's *t* test and considered significant at $p < 0.05$.

Results

Osteocytic (Ocy454) Cell Line Basal and Hormonal Characterization—Our method for osteocyte cell line development coupled fluorescent sorting for an osteocytic marker (*DMP1*) with functional hormonal screening to accurately ensure the cell line possessed the key functional responses of mature osteocytes *in vivo*. Of several preparations, one population of sorted *DMP-GFP*-SV40 large T antigen (Ocy454) cells was selected for further characterization on the basis of its high expression of *SOST* at early time points at the semipermissive temperature. Ocy454 osteocytic cells displayed a dendritic morphology (Fig. 1*A*) similar to other osteocytic cell lines (32, 33) and at 2 weeks at the semipermissive temperature (37 °C) expressed the *DMP1-GFP* transgene (Fig. 1, *B* and *C*).

After 2 weeks at 37 °C, Ocy454 cells expressed significantly higher levels of *SOST* and *DMP1* compared with long bone primary osteocytes as well as the only other available osteocytic cell lines, MLO-Y4 and IDG-SW3 (Fig. 2, *A* and *B*). Upon further study, we also observed that Ocy454 differentiated upon contact inhibition at the permissive temperature (Figs. 1*C* and 2*B*). However, Ocy454 differentiated at a slower pace at the permissive temperature. For example, at the 1-week time point, there were lower levels of *SOST* at the permissive temperature compared with the semipermissive temperature (Fig. 2*B*). In addition, Ocy454 expressed levels of *SOST* that were significantly higher than those expressed by long bone osteoblasts (Fig. 2*B*) as early as 1 week at 37 °C in the absence of differentiation factors. Sclerostin was detected by ELISA in the cell culture supernatant at day 11, and its concentration continued to increase with time in culture (Fig. 2*B*). Furthermore, after 2 weeks at the semipermissive temperature (37 °C), Ocy454 cells expressed high levels of other characteristic osteocytic genes, such as *DMP1* (Fig. 2*B*). In contrast, these cells had low levels of expression of genes characteristic of immature osteocytes and late osteoblasts, such as keratocan (Fig. 2*B*) (42, 43). After 1 week in culture at 37 °C, Ocy454 cells expressed levels of *DMP1* (Fig. 2*B*) that were significantly higher than those expressed by long bone osteoblasts. In addition, *RANKL* was highly expressed at the permissive temperature, and then expression dropped to levels comparable with wild-type osteoblasts and the IDG-SW3 cell line with differentiation at the semipermissive temperature (Fig. 2*B*). Interestingly, the expression of *FGF23* in Ocy454 followed a biphasic pattern of expression with significantly more mRNA at 1 week in semipermissive culture than at later time points (Fig. 2*B*).

We next assessed Ocy454 cell responsiveness to known osteocyte regulators. Short term (4-h) treatment with human (h)PTH(1–34), forskolin, or (16-h) PGE_2 induced a statistically significant down-regulation of *SOST* (Fig. 3*A*; $p < 0.001$ for all) and sclerostin both in whole cell lysate and conditioned medium (Fig. 3, *B* and *C*). These results are consistent with the known inhibitory effects of these agents on *SOST* expression. In contrast, a PGE_2 inhibitor, indomethacin, caused an increase in *SOST* (Fig. 3*B*), showing that Ocy454 cells have an intact hormonal axis that increases *SOST* expression.

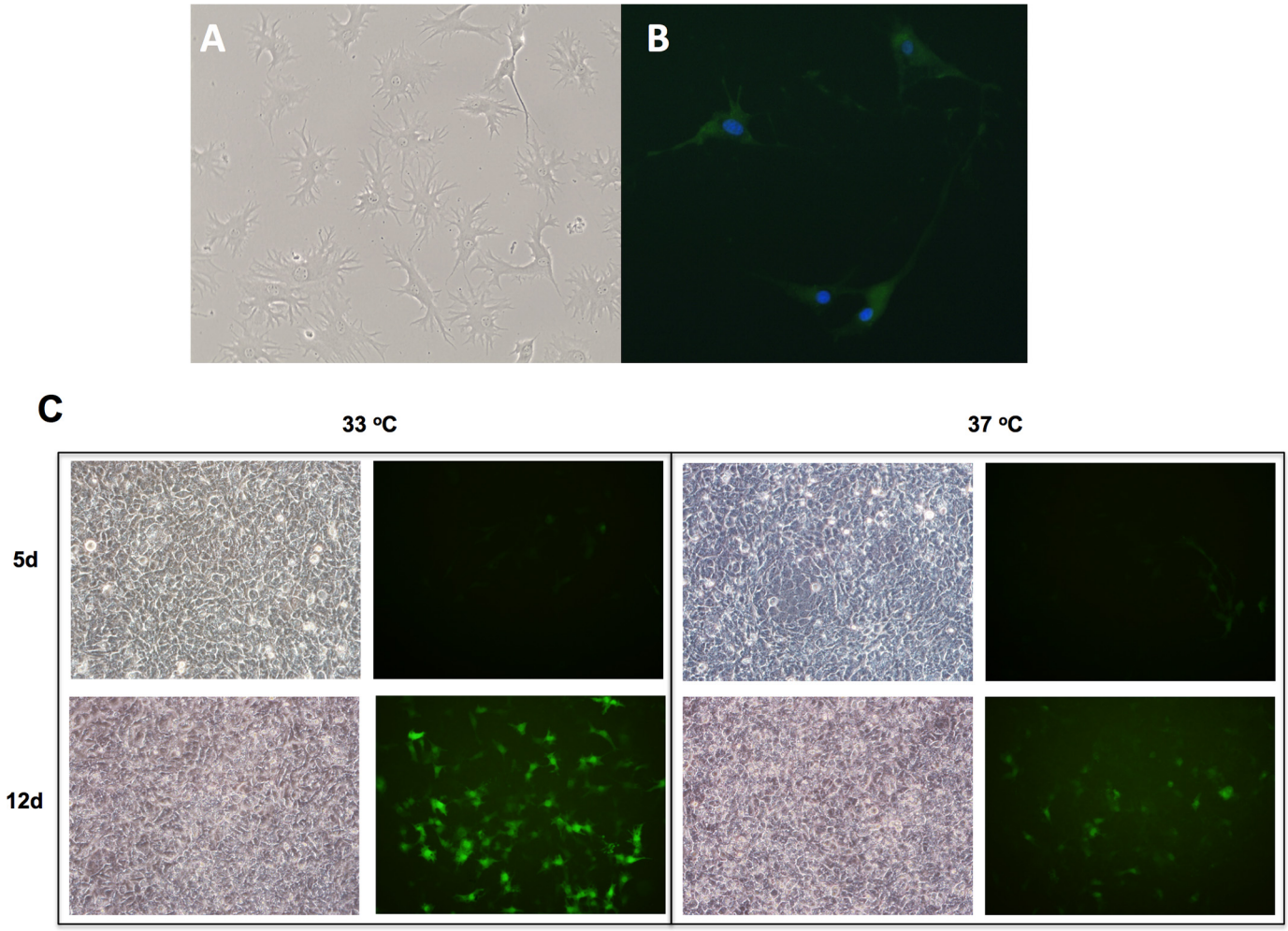

FIGURE 1. *A*, representative dendritic morphology of osteocytic cell line Ocy454. *B*, *DMP1-GFP* expression at 3 days for permissive temperature (33 °C). *C*, *DMP1-GFP* expression time course at 5 and 12 days (*d*) for both permissive (33 °C) and semipermissive temperature (37 °C).

In addition, hPTH(1–34) dose- and time-response experiments showed Ocy454 to be sensitive to down-regulation of *SOST* in as short as 2 h (100 nM; Fig. 3*D*) and a 50% suppression at doses as low as 0.1 nM hPTH(1–34) (Fig. 3*D*). Similarly, hPTH(1–34) (4 h), forskolin, and PGE_2 caused concurrent increases in *RANKL* mRNA (Fig. 3*E*). hPTH(1–34) suppressed *Mef2C* mRNA (Fig. 3*F*), consistent with previous reports (44, 45), and *DMP1* mRNA (Fig. 3*G*). There was no regulation of *FGF23* mRNA by 4-h PTH treatment in Ocy454 at 1 or 2 weeks in two-dimensional non-collagen- and collagen-coated 6-well plate culture conditions (data not shown).

We and others have previously reported that mice lacking (35, 46) $G_s\alpha$ have increased levels of *SOST*/sclerostin. To confirm these *in vivo* results in Ocy454 cells, we used shRNA to knock down $G_s\alpha$ in Ocy454 as was done previously for *HDAC5* (36). The range of sclerostin secretion (normalized to cell number) was determined in each experiment using 10 separate control lentiviruses expressing shRNAs against non-expressed genes (*LacZ*, luciferase, *GFP*, and red fluorescent protein). *Dotted lines* indicate two standard deviations above the mean value of sclerostin secretion (normalized to cell number) in the presence of the control hairpins. As shown in Fig. 4*A*, two of five hairpins tested to achieve lentivirus-mediated shRNA knockdown of *GNAS* (but not related heterotrimeric G-proteins *GNAQ* and *GNA11*) consistently increased sclerostin secretion (individual hairpins labeled next to corresponding data points). The individual hairpins that reduced *GNAS* mRNA levels accordingly increased *SOST* expression (Fig. 4*B*), thereby confirming the expected knockdown/phenotype relationship for this known *SOST* regulator. *GNAS* hairpins "G2" and "G9" both effectively reduced $G_s\alpha$ protein levels (Fig. 4*C*), and hairpin G2 was selected for further study. Sclerostin secretion in control (shLuciferase) and *GNAS* G2 shRNA-expressing cells was determined over time. As shown in Fig. 4*D*, *GNAS* shRNA causes an increase in sclerostin secretion at all time points with the most dramatic results at early times after switching cells from 33 to 37 °C. Finally, *GNAS* shRNA cells were tested for PTH responsiveness. Fig. 4*E* shows that *GNAS* shRNA increases basal *SOST* expression (after 14 days at 37 °C); furthermore, whereas control cells respond to PTH at this time point with suppression of *SOST* levels, this is not the case when $G_s\alpha$ levels are reduced. Taken together, these data confirm a cell-intrinsic role for $G_s\alpha$ in osteocytes and further support the use of Ocy454 cells for studying *SOST* gene regulation.

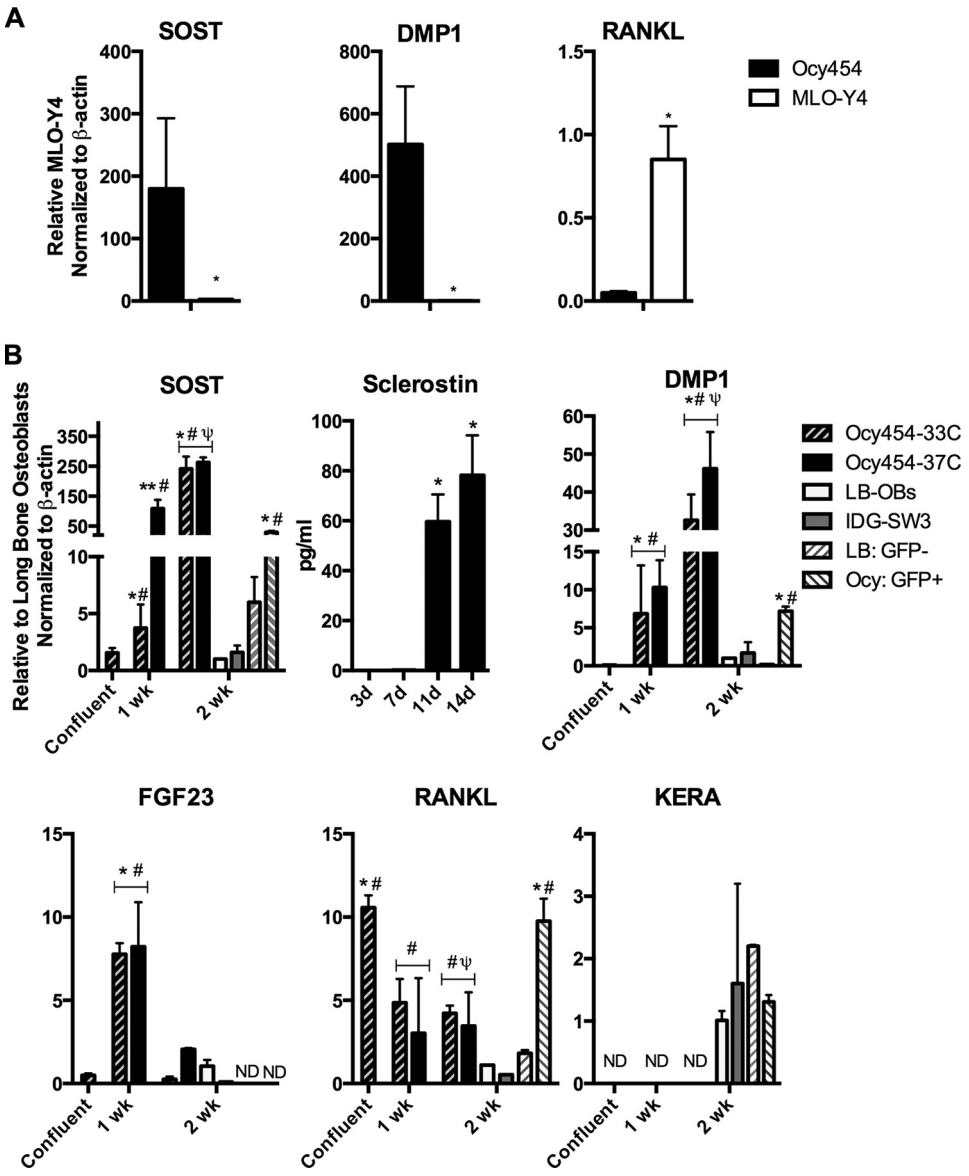

FIGURE 2. *A*, Ocy454 at 2 weeks (37 °C) (*black bars*) express characteristic osteocytic markers *versus* MLO-Y4 in the absence of differentiation medium. *B*, Ocy454 (*Ocy*) at 1 and 2 weeks (*wk*) (37 °C) (*black bars*) express characteristic osteocytic markers *SOST*, sclerostin, *DMP1*, *FGF23*, and *RANKL* and lack keratocan (*KERA*) expression in the absence of differentiation medium compared with long bone osteoblasts (*LB-OBs*), IDG-SW3 (2 weeks), long bone (*LB*) *DMP1-GFP*− and long bone *DMP1-GFP*+ osteocytes. *, $p < 0.001$ for 1 and 2 weeks at semipermissive growth temperature (37 °C) *versus* permissive growth temperature (33 °C; 3 days (*d*)); **, $p < 0.001$ for 1 and 2 weeks at semipermissive temperature *versus* permissive growth temperature at the indicated time points; #, $p < 0.001$ for Ocy454 *versus* long bone osteoblasts; Ψ, $p < 0.001$ for Ocy454 *versus* long bone *DMP1-GFP*+ osteocytes at the indicated time points. *ND*, not detected. *Error bars* represent S.D. of 1.

Three-dimensional Culture Enhances Osteocytic Phenotype—To evaluate the effects of a three-dimensional culture environment on the expression of osteocyte-specific genes and to provide a scaffold for cell attachment in the rotating wall bioreactor system used to simulate microgravity, Ocy454 cells were seeded onto scaffolds and cultured for an additional 7–14 days. Consistent with our two-dimensional culture results, we also observed a significant down-regulation of *SOST* (Fig. 5*A*), increases in *RANKL* (Fig. 5*B*), and decreases in *DMP1* (Fig. 5*D*) in three-dimensional cultures ($p < 0.001$ for all) upon PTH treatment. Previous reports have demonstrated that TGFβ_1 increases *SOST*/sclerostin levels during mechanical loading (47, 48). In contrast to prior reports, treatment of Ocy454 cells with TGFβ_1 (10 ng/ml; 24 h) resulted in a down-regulation of *SOST* (Fig. 5*A*) and increases in *RANKL* (Fig. 5*B*), and a known TGFβ_1-responsive gene, *Serpine1*, increased 2.3 ± 0.1-fold ($p < 0.007$). Interestingly, in contrast to two-dimensional cultures, culture in three dimensions with 4-h PTH treatment resulted in a 5-fold ($p < 0.001$) increase in *FGF23* expression (Fig. 5*C*). In a direct comparison between three-dimensional and two-dimensional culture at an early time point (3 days at 37 °C), Ocy454 had significantly higher amounts of *SOST* and *RANKL* in the three-dimensional culture conditions (Fig. 5*G*) than in the two-dimensional setting. Furthermore, Ocy454 displayed dendritic morphology in three-dimensional culture conditions (Fig. 5*E*), and we observed decreases in sclerostin protein expression with hPTH(1–34) treatment in three-dimensional culture (Fig. 5*F*).

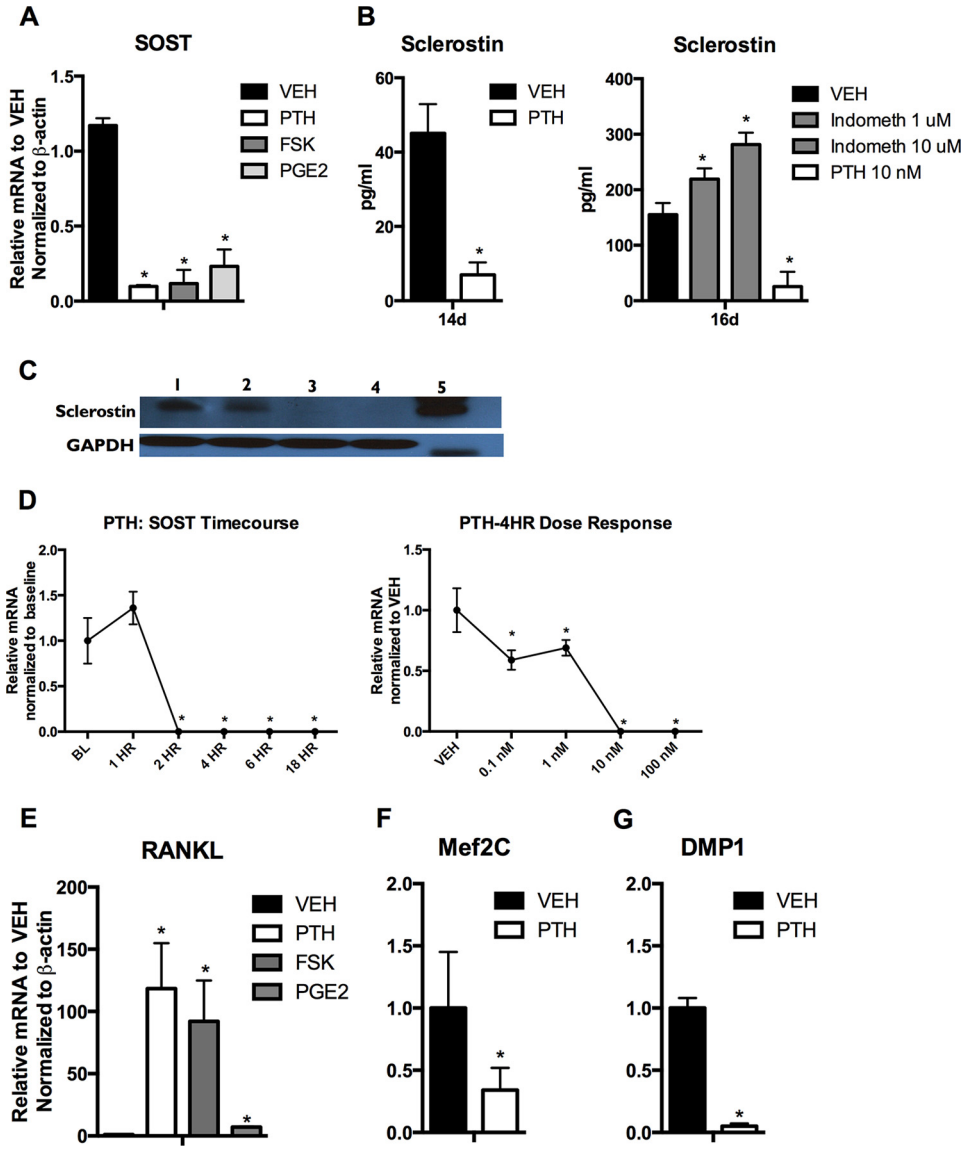

FIGURE 3. *A*, Ocy454 cells show decreased *SOST* expression after treatment with PTH(1–34) (4 h, 100 nM), forskolin (4 h, 10 μM), PGE2 (16 h, 100 nM) at 2 weeks at semipermissive temperature. *B*, 16-h hPTH(1–34) (100 nM) treatment decreases secreted sclerostin as measured by ELISA (ALPCO), and 48-h indomethacin (*Indometh*) treatment (1 and 10 μM) increases secreted sclerostin by ELISA (Amgen). *C*, 4-h hPTH(1–34) (100 nM) treatment of Ocy454 at 2 weeks suppresses total cell lysate sclerostin. *Lanes 1* and *2*, vehicle (*VEH*); *lanes 3* and *4*, hPTH(1–34); *lane 5*, sclerostin standard (APLCO). *D*, hPTH(1–34) time course and dose response for *SOST* suppression. *E*, 4-h treatment to hPTH(1–34), forskolin, and 16-h PGE_2 increases *RANKL* at 2 weeks. Four-hour hPTH(1–34) treatment suppresses *Mef2C* (*F*) and *DMP1* (*G*). *, $p < 0.001$ for all *SOST* time courses and hormone/cytokine treatments *versus* vehicle. *Error bars* represent S.D. of 1. *d*, days.

Fluid Shear Stress Regulation of Ocy454 in Two-dimensional Culture—Ocy454 were then subjected to continuous unidirectional fluid shear stress in two-dimensional culture conditions. Consistent with previous reports using UMR 106.01 osteoblast-like cells (39), short term (2-h) fluid shear stress significantly suppressed *SOST* mRNA levels at low and high shear stresses (Fig. 6*A*). Whereas *RANKL* was reduced at low shear stress (0.5–2 dynes/cm^2), *RANKL* and *DMP1* were increased at higher shear stress (8 dynes/cm^2) as shown in Fig. 6, *B* and *C*. These results demonstrate that Ocy454 cells are exquisitely responsive to mechanical forces with intact *SOST*, *DMP1*, and *RANKL* regulation to overloading stimuli. Our results also suggest differential regulation of *SOST* and *DMP1* to fluid shear stress but not to simulated microgravity, whereas the response to hPTH(1–34) is the same.

Simulated Microgravity Increases SOST/Sclerostin and RANKL—We then utilized the NASA-developed rotating wall bioreactor system to mimic microgravity to assess whether osteocytes can directly sense mechanical unloading and regulate the expression of sclerostin and *RANKL*, which are known be involved in the response of bone to unloading. Indeed, under simulated microgravity conditions (3 days), there was a statistically significant increase of 3.5 ± 1.9-fold ($p < 0.001$) in *SOST* expression compared with static controls (Fig. 7*A*). Secreted sclerostin as assessed by ELISA was also increased by 1.4 ± 0.1 as early as 1 day, 2.7 ± 0.4 at 2 days, and 4.7 ± 0.1 at 3 days ($p < 0.001$ for all) (Fig. 7*B*). There were no significant changes in other osteoblastic genes (osteocalcin, alkaline phosphatase, and osterix mRNAs) between the loaded and unloaded bioreactors, demonstrating that the increase in

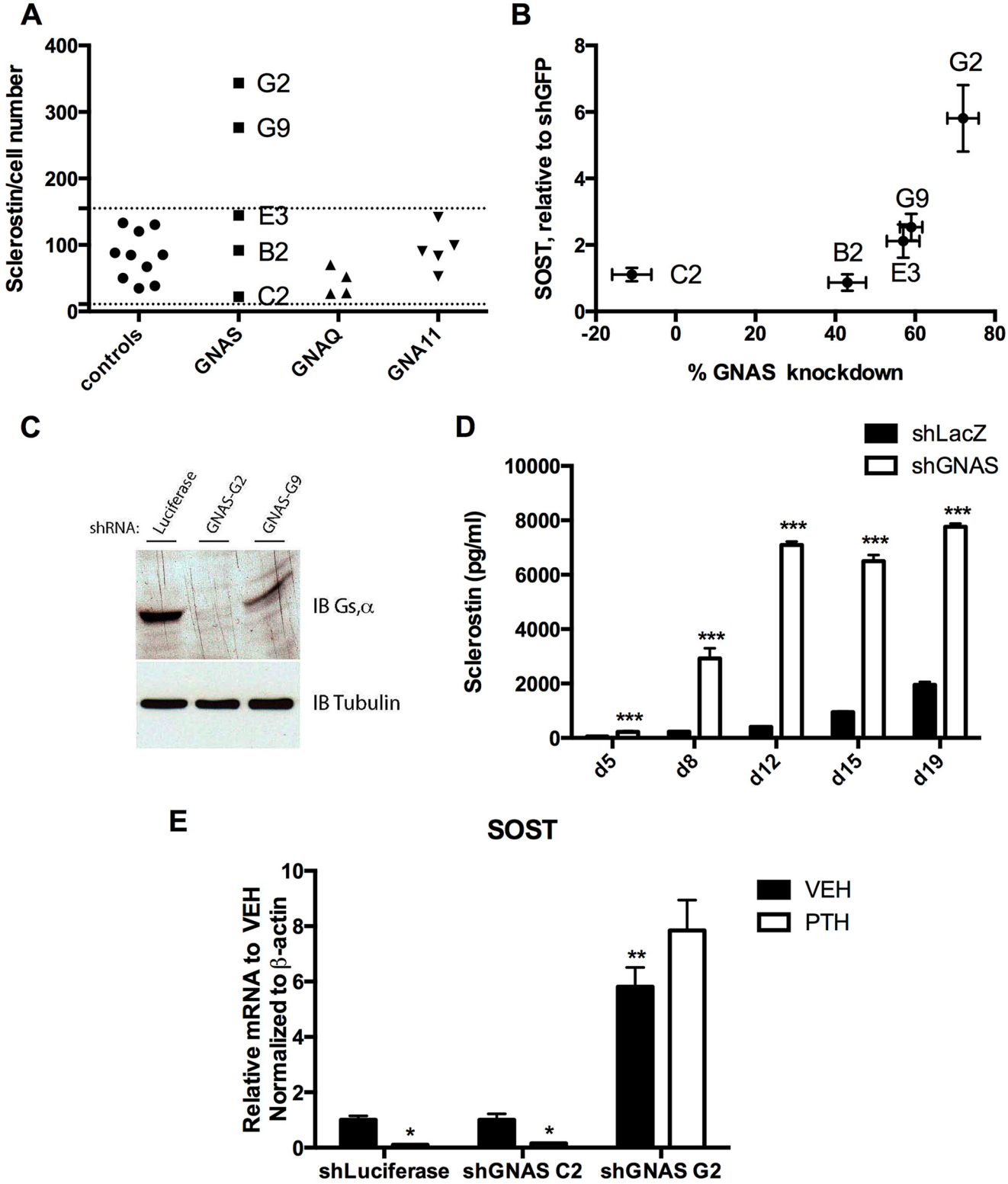

FIGURE 4. *A*, Ocy454 cells were infected with control shRNA-expressing lentiviruses (sh*GFP*, shLuciferase, shRed fluorescent protein, and sh*LacZ*) and five separate hairpins targeting the indicated gene. Each data point represents sclerostin/cell number values obtained for an individual hairpin. *Dotted lines* indicate values two standard deviations above and below those of the controls. For *GNAS*, individual hairpins are labeled on the data plot. *B*, Ocy454 cells were infected with shGFP and the indicated *GNAS* shRNA lentiviruses and then switched to 37 °C. 14 days later, RNA was isolated, and RT-quantitative PCR was performed for β-actin, *GNAS*, and *SOST*. *C*, as in *B* except lysates were generated for immunoblotting. *D*, as in *B* except conditioned medium was collected at the indicated times for sclerostin ELISA. *E*, as in *B* expect cells were treated with vehicle or hPTH(1–34) (50 nM) for 4 h followed by semi-quantitative PCR for *SOST* and β-actin. *, $p < 0.01$ for hPTH(1–34) *versus* vehicle (*VEH*); **, $p < 0.001$ for sh*GNAS* G2 *versus* shLuciferase and sh*GNAS* C2; ***, $p < 0.001$ for sh*GNAS versus* sh*LacZ* for all time points. *Error bars* represent one S.D.

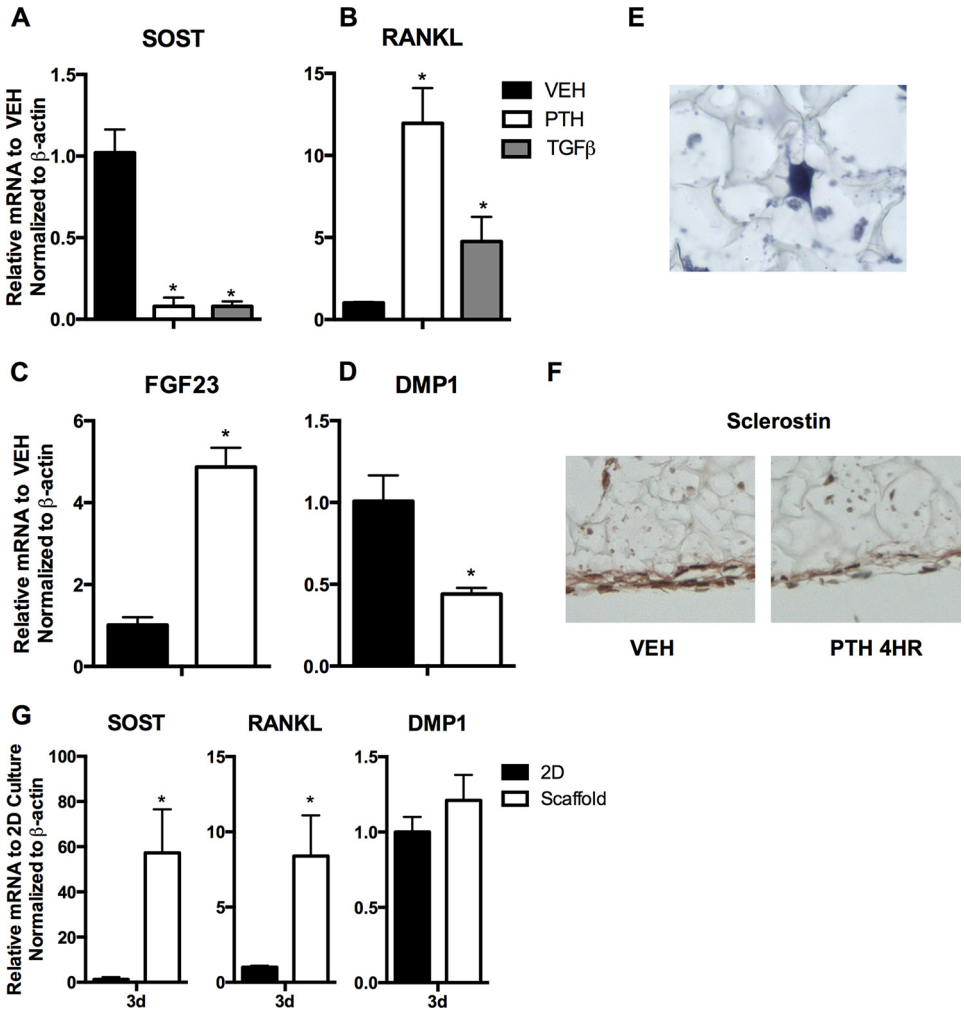

FIGURE 5. Ocy454 cells were grown on collagen-coated (*A–D*) three-dimensional scaffold (for hPTH(1–34) experiments). Four-hour hPTH(1–34) (100 nM) and 24-h TGFβ_1 (10 ng/ml) treatment at 12–14 days decreases *SOST* (*A*) and increases *RANKL* (*B*). Four-hour hPTH(1–34) increases *FGF23* (*C*) and decreases *DMP1* (*D*) expression. *E*, representative H&E stain of Ocy454 cell within the scaffold. *F*, 4-h hPTH(1–34) (100 nM) treatment decreases sclerostin expression of Ocy454 cells on the scaffold. *G*, Ocy454 gene expression for *SOST*, *DMP1*, and *RANKL* on three-dimensional scaffolds *versus* two-dimensional (*2D*) culture at semipermissive growth temperature for 3 days (*d*) (37 °C). *, $p < 0.001$ for hPTH(1–34) or $p < 0.007$ for TGFβ_1 *versus* vehicle (*VEH*). *Error bars* represent S.D. of 1.

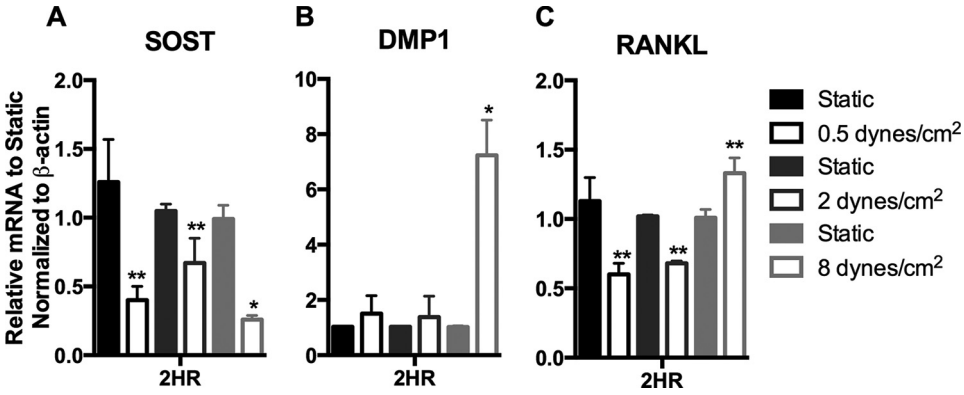

FIGURE 6. Short term (2-h) fluid shear stress in two-dimensional culture reduces *SOST* (*A*), increases *DMP1* at high shear stress (8 dynes/cm^2) (*B*), and reduces *RANKL* at low shear stress (0.5–2 dynes/cm^2) and increases *RANKL* at high shear stress (8 dyne/cm^2) (*C*). *, $p < 0.001$; **, $p < 0.05$ for static *versus* fluid shear stress. *Error bars* represent S.D. of 1.

SOST/sclerostin expression was not a consequence of an altered cell state as we observed in our prolonged two-dimensional fluid shear stress experiments. In an effort to identify upstream regulator of *SOST*/sclerostin expression, we assessed changes in reported and potential regulators of *SOST* in the *Mef2* pathway (*Mef2A–D*), PGE_2 pathway (*mPTGES-1*, *15-HGPD*, *EP2*, and *EP4*), *SIRT1*, osterix, *PTHrP*, PTH receptor, and periostin. We observed no changes in mRNA levels for any of these known regulators of *SOST* (Table 2) following simulated microgravity.

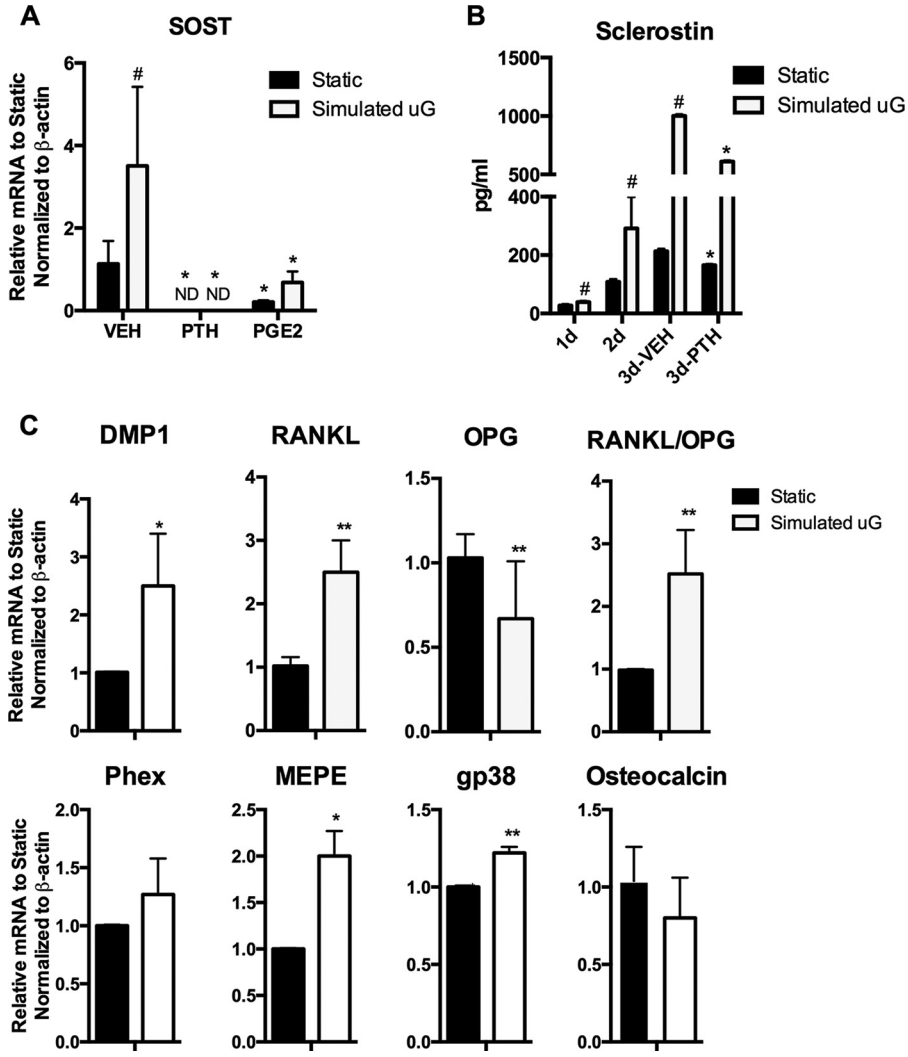

FIGURE 7. *A*, 3-day simulated microgravity (*white bars*) increases *SOST* compared with static controls (*black bars*), and 4-h hPTH(1–34) (50 nM) and 16-h PGE_2 (5 nM) decrease *SOST* in both simulated microgravity (*uG*) and static controls. *B*, sclerostin increases as early as 1 day (*d*) of exposure to simulated microgravity and remains elevated through 3 days. Overnight (16-h) hPTH(1–34) (50 nM) treatment on days 2–3 suppresses secreted sclerostin as measured by ELISA (APLCO). *C*, 3-day simulated microgravity increases *DMP1*, *RANKL*, *RANKL*/*OPG* ratio, *gp38*, and *MEPE*; decreases *OPG*; and has no effect on *Phex* or osteocalcin. #, $p < 0.001$; **, $p < 0.05$ for simulated microgravity *versus* static controls; *, $p < 0.001$ for all hormone/cytokine treatments *versus* vehicle (*VEH*). *ND*, not detected. *Error bars* represent S.D. of 1.

Consistent with previous reports of osteoblasts increasing *RANKL* expression in simulated microgravity conditions (49), we observed increased *RANKL* mRNA (Fig. 7*C*) and a concurrent modest reduction in *OPG* mRNA (Fig. 7*C*), resulting in a statistically significant increase in the *RANKL*/*OPG* ratio in unloaded *versus* static conditions (Fig. 7*C*). We also detected a modest increase on mRNAs encoding *DMP1*, *MEPE*, and *gp38* with no change in *Phex* or osteocalcin mRNA under simulated microgravity conditions (Fig. 7*C*). Thus, we report these regulatory changes to osteocytic genes as a signature of osteocytes exposed to simulated microgravity.

G-protein-coupled Receptor Responsiveness: SOST/Sclerostin in Simulated Microgravity—To determine whether activation of PTH receptors (or other G-protein-coupled receptors) could still suppress *SOST*/sclerostin in microgravity, we tested the effects of PTH and PGE_2 treatment in simulated microgravity. PTH (Fig. 7*A*) suppressed *SOST* and sclerostin levels of expression (Fig. 7*B*) to the same extent in static and unloaded conditions ($p < 0.001$). Similarly, PGE_2 caused the same magnitude of suppression of *SOST* expression in both static and simulated microgravity conditions. These results demonstrate that, although the increase in *SOST* expression is not dependent on reductions in G-protein-coupled receptor expression (PTH receptor and EP2/4) or $G_s\alpha$ activity (Table 2), modulating G-protein-coupled receptor signaling can still regulate *SOST*/sclerostin expression in the setting of microgravity or unloading, such as disuse.

Long Term Fluid Shear Stress Regulation of Ocy454—One limitation of the NASA rotating wall bioreactor system is the possible generation of minimal fluid shear stress demonstrated to be on the order of 0.5–2 dynes/cm^2 (38, 50). To investigate whether the changes in gene expression observed in the NASA bioreactor were indeed due to simulated microgravity and not minimal shear stress, we subjected Ocy454 cells to long term exposure (1 or 3 days) to low laminar fluid shear stresses (0.5–2 dynes/cm^2) in three-dimensional (Alvetex) culture condi-

TABLE 2
Evaluated regulators of SOST/sclerostin in simulated microgravity

ECR5 enhancers
Mef2A, *-C*, *-D*; *Mef2B* (not expressed) (34, 45, 67)
***SOST* promoter transcription factors**
TFGB1 (47, 48)
Osterix (59)
Runx2 (68)
SIRT1 (58)
Pax6 (51)
Periostin (44)
MyoD: not expressed (68)
$G_s\alpha$ (35, 46)
PGE_2 pathway
EP2, *EP4* (54, 56)
Cox-2
mPTGES-1
15-HGPD
Cell membrane receptors
PTH1R
PTHrP: not expressed
P2XR1–7

tions. At 2 dynes/cm^2, we observed a significant reduction in *SOST* mRNA and no change in *DMP1* mRNA at 1 day (Fig. 8). At 0.5 dyne/cm^2, we observed significant suppression of *SOST* mRNA; a significant increase in *DMP1* mRNA; and decreases in *OPG*, *MEPE*, *gp38* (1 day), and osteocalcin mRNAs with no effect on *RANKL* or *Phex* mRNA (Fig. 8). Similar results for 2 dynes/cm^2 were observed at 3 days (Fig. 8) with the exception of a lack of regulation of *DMP1* mRNA. These data clearly indicated that the up-regulation of *SOST*/sclerostin present in the NASA rotating wall bioreactor system was indeed due to simulated microgravity and not minimal shear stress.

In addition, as shown in Fig. 9, we subjected Ocy454 to two-dimensional long term low fluid flow. These low flow conditions induced changes in the differentiation state of Ocy454 as illustrated by significantly elevated levels of expression of *SOST*, *DMP1*, *RANKL*, *OPG* (3 days), *Phex*, *MEPE*, and *gp38* with a reduction of osteocalcin expression (Fig. 9). Overall, these two-dimensional and three-dimensional long term mechanical overloading results demonstrated that our simulated microgravity experiments reflect a unique osteocyte cellular response to mechanical underloading stimuli.

Discussion

The primary objective of this study was to determine whether increases in *SOST*/sclerostin and *RANKL* seen in the context of disuse-induced bone loss are an intrinsic osteocytic response to mechanical unloading. Although it has been established that osteocytes are key players in the response of bone to mechanical stimuli (10, 39, 40, 52, 53), it is still unclear whether their response to unloading is a direct response to reduction in load as theorized by Wolff's law or a consequence of changes in systemic endocrine or paracrine factors. Furthermore, the biochemical response of the osteocytic network to overloading (10, 39, 40) does not in it of itself provide evidence for a direct response to unloading stimuli. Here we present new data showing that osteocytes elicit an intrinsic response to mechanical loading that is independent of the known external hormonal influence of PTH and other factors.

Prior studies in rodents have reported increases in *SOST*/sclerostin in bone tissue (10) and in circulating sclerostin (19) during unloading. In addition, increased circulating serum sclerostin levels with a concurrent reduction of PTH levels have been reported in the context of disuse-induced bone loss in rodents (55) and humans (17). However, as PTH is a strong negative regulator of *SOST*/sclerostin, these *in vivo* studies cannot address the question of whether osteocytes can directly sense mechanical unloading or respond to hormonal changes.

Importantly, our results suggest that the increase in bone resorption in mechanical unloading and microgravity with associated transient hypercalcemia and reduced parathyroid hormone levels is not the driving force for increases in *SOST*/sclerostin and *RANKL* expression. Thus, for the first time, we have observed isolated osteocytes sensing mechanical unloading and responding with increases in *SOST*/sclerostin and the *RANKL*/*OPG* ratio.

The transcriptional regulators of *SOST*/sclerostin in mechanical unloading are currently unknown. However, *Mef2* transcription factors have been shown in several contexts to bind a distal enhancer (ECR5) in the *SOST* locus, resulting in the increased expression of *SOST*/sclerostin (34, 45). However, we observed no transcriptional changes in the potential regulators of *SOST* in the *Mef2* pathway (*Mef2A*, *-C*, and *-D*) (Table 2). Furthermore, because PGE_2 is a known negative regulator of *SOST*/sclerostin in a *Mef2*-independent mechanism (56) and reductions in PGE_2 production genes (*Cox-2*) have been observed in osteoblasts exposed to microgravity (57), we assessed changes in the PGE_2 production and degradation pathways (*mPTGES-1* and *15-HGPD*) and receptor expression (*EP2* and *EP4*) as shown in Table 2. Notably, no changes in mRNA of transcripts responsible for PGE_2 production, PGE_2 degradation, or PGE_2 receptors were observed between static and unloaded cultures, implying that the increases of *SOST*/sclerostin in mechanical unloading are presumably not arising from changes in the PGE_2 pathway. Several transcription factors have also been reported to suppress the *SOST* promoter (like *SIRT1* and osterix) (58, 59) or act at the distal enhancer (ECR5) (like $TGF\beta_{1-3}$) (47). However, in the context of mechanical unloading, we observed no change in *SIRT1*, osterix, or $TGF\beta_{1-3}$ mRNAs (Table 2). It has also been proposed that the periostin matricellular protein suppresses *SOST* in a *Mef2C*-dependent mechanism that is regulated by PTH (44, 60). However, in Ocy454, we observed no correlation among sclerostin, PTH, and periostin mRNA or protein expression in two-dimensional cultures or in the context of mechanical unloading (data not shown). Thus, future studies investigating the novel transcriptional or post-transcriptional regulation of *SOST*/sclerostin the context of mechanical unloading and microgravity are warranted.

G-protein-coupled hormonal (PTH) and cytokine regulators (PGE_2) were capable of suppressing the increases of *SOST*/sclerostin seen in mechanical unloading. Thus, although our results show that osteocytes can directly sense mechanical unloading, they also suggest that the overall level of sclerostin *in vivo* appears to be an integral response of the osteocyte network to mechanical loading, hormonal, and cytokine cues. Of particular note, we have shown that mice lacking PTH receptor in osteocytes lose bone in the hind limb unloading model, consistent with our *in vitro* findings that G-protein-coupled receptor

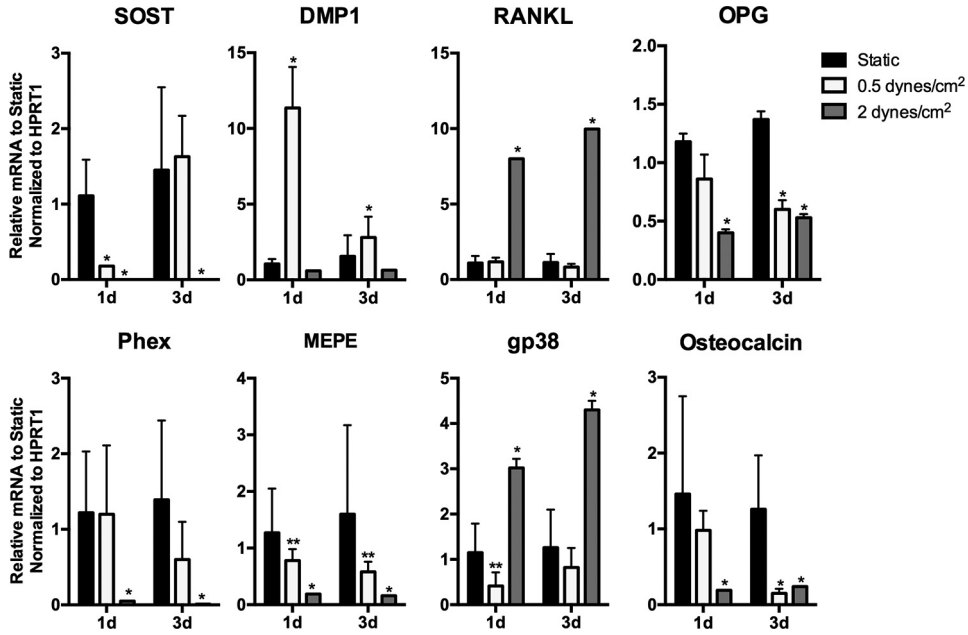

FIGURE 8. **Fluid shear stress of Ocy454 in three-dimensional culture at 1 and 3 days (*d*).** Fluid low shear stress of 0.5 and 2 dynes/cm^2 reduces *SOST* (*A*); increases *DMP1* (*B*); decreases *OPG* (*C*), *Phex* (*D*), and *MEPE* (*E*); increases *gp38* (*F*), and decreases osteocalcin (*G*) at the shear stresses and time points indicated. *, $p < 0.001$; **, $p < 0.05$ for static *versus* fluid shear stress. *Error bars* represent S.D. of 1.

signaling may play a minimal role in disuse-induced bone loss. One study has recently reported that *SOST* regulation in mechanical unloading in rodents could be site-specific with modest (−1.5%) down-regulation in cancellous metaphyseal and cortical bone, whereas up-regulation was seen in diaphyseal cortical (61) regions. Our results are consistent with these findings as our cell lines were isolated from the diaphysis of long bones. However, as the majority of osteocytes in the load-bearing skeleton are located in the diaphysis of long bones and circulating levels of sclerostin are elevated in the setting of disuse-induced bone loss, the clinical significance of the heterogeneic nature of the osteocytic network remains to be further explored. Furthermore, although the NASA rotating wall bioreactor provides a solid body rotation with a minimal fluid shear stress in the range of 0.5–2 dynes/cm^2 38, 50, no currently existing *in vitro* ground-based model of microgravity can fully eliminate the low level of shear stress inherent in our model.

However, short mechanical loading (10, 62) and fluid shear stress (39) are known to cause decreased, not increased, levels of *SOST*/sclerostin and *RANKL* as we have observed (Fig. 7). To further investigate this confounding variable of minimal fluid shear stress in the NASA bioreactor, we subjected Ocy454 cells in two-dimensional and three-dimensional culture conditions to low unidirectional fluid shear stress. Importantly, neither two-dimensional nor three-dimensional fluid shear stress matched the pattern of osteocytic gene expression seen in simulated microgravity. In addition, cells on the surfaces of the scaffolds are likely exposed to shear stresses higher in range than cells within the scaffold. However, the same seeding technique was used in all scaffold experiments so non-uniformity in cell distribution could in and of itself not account for the significant down-regulation of *SOST* in three-dimensional fluid flow (Fig. 8) compared with the increase in *SOST* (Fig. 7) we observed in the simulated microgravity experiments. Finally, additional variables, such as nutrient availability, could also be acting as confounding factors to our observed results. However, the simulated microgravity experiments utilized a 110-ml bioreactor. Daily changes of 10% volume of medium were also performed to facilitate elimination of bubbles. Thus, for the cell density and number, these culture conditions for both static and microgravity conditions are nutrient-rich. Our interpretation notwithstanding, we acknowledge that such confounding variables specific to osteocytic cell cultures in simulated microgravity will need to be addressed in future experiments under conditions of true microgravity.

To enable these studies, we generated a novel osteocytic cell line Ocy454 that recapitulates known *in vivo* osteocytic functions without the requirement for long term high density cultures and in the absence of differentiation medium. These cells were isolated from long bones of double transgenic mice expressing both a *GFP* under the *DMP1* promoter and a temperature-sensitive large T antigen. These cells can be cultured for a long period of time at permissive conditions (33 °C) without losing their phenotypic characteristics and then can rapidly recapitulate a mature osteocytic phenotype after 10–12 days in culture at semipermissive conditions (37 °C). As expected for an osteocyte, these cells express high levels of *SOST*/sclerostin, *DMP1*, *Phex*, and *E11*, whereas they have undetectable levels of the osteoblastic marker keratocan at all time points. Thus, in contrast to currently available osteocytic cell lines (MLO-Y4 and IDG-SW3 for example), the uniqueness of these cells is their expression of mature osteocytic genes in the absence of differentiation factors at early time points, suggesting that these cells display a mature osteocytic phenotype in a shorter experimental time frame. In addition, Ocy454 responded to short term mechanical overloading, achieved via both traditional two-dimensional laminar shear stress and three-di-

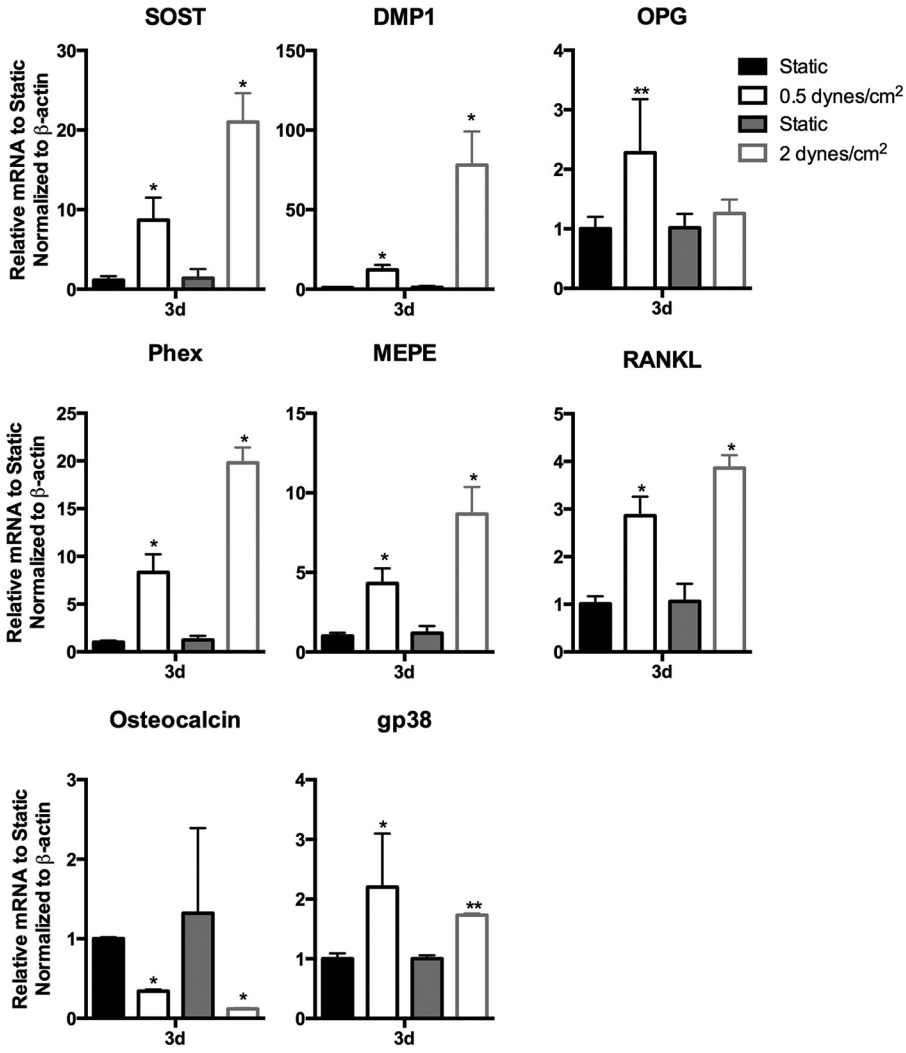

FIGURE 9. **Long term (3-day) fluid shear stress in two-dimensional culture increases *SOST*, *DMP1*, *RANKL*, *OPG*, *Phex*, *MEPE*, and *gp38* and decreases osteocalcin at the indicated shear stresses and time points.** *, $p < 0.001$; **, $p < 0.05$ for static *versus* fluid shear stress. *Error bars* represent S.D. of 1.

mensional fluid shear stress, by reducing *SOST* as reported previously (39).

Interestingly, *RANKL* expression is higher at permissive conditions (more undifferentiated state), and this expression rapidly declines upon differentiation (2–3 days at 37 °C), suggesting that high *RANKL*-expressing cells might belong to a less mature "osteocytic" phenotype. Similar findings were evident for *FGF23* as well. In addition, consistent with prior reports that osteocytes have improved characteristics in three-dimensional culture conditions (63, 64), our osteocytic cell line exhibited increased *FGF23* upon PTH treatment in three-dimensional culture conditions but not two-dimensional culture conditions. It is well appreciated that for a wide variety of cell types three-dimensional cell cultures mimic to a greater degree the *in vivo* conditions by preserving the three-dimensional integrity of individual cells, allowing for cell aggregation and direct signaling and enabling cells to create their own niche microenvironment in conjunction with their extracellular matrix (65). Thus, our studies add to the growing body of evidence for the use of three-dimensional *in vitro* culture conditions to study certain aspects of osteocyte biology. For the experiments we have conducted, our cell line faithfully reflects key characteristics of *bona fide in vivo* osteocytes.

In addition, we have also isolated another long bone cell line (Ocy491) (66) using this same technique, but it has the characteristics of a less mature osteocyte, requiring up to 21 days to produce appreciable levels of *SOST*, that could be useful for osteoblast-to-osteocyte differentiation studies. Thus, here we report the establishment of osteocyte cell lines that can be routinely cultured over short time periods with high level expression of *SOST*/sclerostin that is responsive to hormonal (PTH), cytokine, and mechanical stimuli, enabling a wide diversity of future studies on the regulation of mature osteocytes in other disease processes.

In conclusion, isolated osteocytes can directly sense a mechanical unloading stimulus, resulting in the increases in expression of both inhibitors of bone formation (*SOST*/sclerostin) and stimulators of bone resorption (notably *RANKL* and the *RANKL*/*OPG* ratio). Future therapies, aimed at modulating the gravity-sensing pathways of the osteocyte could lead to improved therapies for a range of bone disorders.

Acknowledgments—We acknowledge Dr. Stefan Przyborski for technical support of this work. We thank Drs. John Doench and David Root of the Broad Institute of Harvard and Massachusetts Institute of Technology (Cambridge, MA) for providing shRNA reagents and protocols; Dr. Lynda Bonewald for providing the MLO-Y4 and IDG-SW3 cell lines; and Drs. Julie Hughes, Stephen Muza, and Ronald Wayne Matheny for facilitating use of the Flexcell Streamer for this project.

References

1. Spector, E. R., Smith, S. M., and Sibonga, J. D. (2009) Skeletal effects of long-duration head-down bed rest. *Aviat. Space Environ. Med.* **80,** A23–A28
2. LeBlanc, A. D., Spector, E. R., Evans, H. J., and Sibonga, J. D. (2007) Skeletal responses to space flight and the bed rest analog: a review. *J. Musculoskelet. Neuronal Interact.* **7,** 33–47
3. Morse, L. R., Sudhakar, S., Danilack, V., Tun, C., Lazzari, A., Gagnon, D. R., Garshick, E., and Battaglino, R. A. (2012) Association between sclerostin and bone density in chronic spinal cord injury. *J. Bone Miner. Res.* **27,** 352–359
4. Inniss, A. M., Rice, B. L., and Smith, S. M. (2009) Dietary support of long-duration head-down bed rest. *Aviat. Space Environ. Med.* **80,** A9–14
5. Stein, E. M., Carrelli, A., Young, P., Bucovsky, M., Zhang, C., Schrope, B., Bessler, M., Zhou, B., Wang, J., Guo, X. E., McMahon, D. J., and Silverberg, S. J. (2013) Bariatric surgery results in cortical bone loss. *J. Clin. Endocrinol. Metab.* **98,** 541–549
6. Vilarrasa, N., San José, P., García, I., Gómez-Vaquero, C., Miras, P. M., de Gordejuela, A. G., Masdevall, C., Pujol, J., Soler, J., and Gómez, J. M. (2011) Evaluation of bone mineral density loss in morbidly obese women after gastric bypass: 3-year follow-up. *Obes. Surg.* **21,** 465–472
7. Sinha, N., Shieh, A., Stein, E. M., Strain, G., Schulman, A., Pomp, A., Gagner, M., Dakin, G., Christos, P., and Bockman, R. S. (2011) Increased PTH and 1.25$(OH)_2$D levels associated with increased markers of bone turnover following bariatric surgery. *Obesity* **19,** 2388–2393
8. Chen, J. H., Liu, C., You, L., and Simmons, C. A. (2010) Boning up on Wolff's law: mechanical regulation of the cells that make and maintain bone. *J. Biomech.* **43,** 108–118
9. Nakashima, T., Hayashi, M., Fukunaga, T., Kurata, K., Oh-Hora, M., Feng, J. Q., Bonewald, L. F., Kodama, T., Wutz, A., Wagner, E. F., Penninger, J. M., and Takayanagi, H. (2011) Evidence for osteocyte regulation of bone homeostasis through RANKL expression. *Nat. Med.* **17,** 1231–1234
10. Robling, A. G., Niziolek, P. J., Baldridge, L. A., Condon, K. W., Allen, M. R., Alam, I., Mantila, S. M., Gluhak-Heinrich, J., Bellido, T. M., Harris, S. E., and Turner, C. H. (2008) Mechanical stimulation of bone *in vivo* reduces osteocyte expression of Sost/sclerostin. *J. Biol. Chem.* **283,** 5866–5875
11. Rodionova, N. V., Oganov, V. S., and Zolotova, N. V. (2002) Ultrastructural changes in osteocytes in microgravity conditions. *Adv. Space Res.* **30,** 765–770
12. Tatsumi, S., Ishii, K., Amizuka, N., Li, M., Kobayashi, T., Kohno, K., Ito, M., Takeshita, S., and Ikeda, K. (2007) Targeted ablation of osteocytes induces osteoporosis with defective mechanotransduction. *Cell Metab.* **5,** 464–475
13. Xiong, J., Onal, M., Jilka, R. L., Weinstein, R. S., Manolagas, S. C., and O'Brien, C. A. (2011) Matrix-embedded cells control osteoclast formation. *Nat. Med.* **17,** 1235–1241
14. Holdsworth, G., Slocombe, P., Doyle, C., Sweeney, B., Veverka, V., Le Riche, K., Franklin, R. J., Compson, J., Brookings, D., Turner, J., Kennedy, J., Garlish, R., Shi, J., Newnham, L., McMillan, D., Muzylak, M., Carr, M. D., Henry, A. J., Ceska, T., and Robinson, M. K. (2012) Characterization of the interaction of sclerostin with the low density lipoprotein receptor-related protein (LRP) family of Wnt co-receptors. *J. Biol. Chem.* **287,** 26464–26477
15. Semënov, M., Tamai, K., and He, X. (2005) SOST is a ligand for LRP5/LRP6 and a Wnt signaling inhibitor. *J. Biol. Chem.* **280,** 26770–26775
16. Paszty, C., Turner, C. H., and Robinson, M. K. (2010) Sclerostin: a gem from the genome leads to bone-building antibodies. *J. Bone Miner. Res.* **25,** 1897–1904
17. Spatz, J. M., Fields, E. E., Yu, E. W., Divieti Pajevic, P., Bouxsein, M. L., Sibonga, J. D., Zwart, S. R., and Smith, S. M. (2012) Serum sclerostin increases in healthy adult men during bed rest. *J. Clin. Endocrinol. Metab.* **97,** E1736–E1740
18. Lin, C., Jiang, X., Dai, Z., Guo, X., Weng, T., Wang, J., Li, Y., Feng, G., Gao, X., and He, L. (2009) Sclerostin mediates bone response to mechanical unloading through antagonizing Wnt/β-catenin signaling. *J. Bone Miner. Res.* **24,** 1651–1661
19. Spatz, J. M., Ellman, R., Cloutier, A. M., Louis, L., van Vliet, M., Suva, L. J., Dwyer, D., Stolina, M., Ke, H. Z., and Bouxsein, M. L. (2013) Sclerostin antibody inhibits skeletal deterioration due to reduced mechanical loading. *J. Bone Miner. Res.* **28,** 865–874
20. Armamento-Villareal, R., Sadler, C., Napoli, N., Shah, K., Chode, S., Sinacore, D. R., Qualls, C., and Villareal, D. T. (2012) Weight loss in obese older adults increases serum sclerostin and impairs hip geometry but both are prevented by exercise training. *J. Bone Miner. Res.* **27,** 1215–1221
21. Gaudio, A., Pennisi, P., Bratengeier, C., Torrisi, V., Lindner, B., Mangiafico, R. A., Pulvirenti, I., Hawa, G., Tringali, G., and Fiore, C. E. (2010) Increased sclerostin serum levels associated with bone formation and resorption markers in patients with immobilization-induced bone loss. *J. Clin. Endocrinol. Metab.* **95,** 2248–2253
22. Bishop, K. A., Coy, H. M., Nerenz, R. D., Meyer, M. B., and Pike, J. W. (2011) Mouse Rankl expression is regulated in T cells by c-Fos through a cluster of distal regulatory enhancers designated the T cell control region. *J. Biol. Chem.* **286,** 20880–20891
23. Smith, S. M., McCoy, T., Gazda, D., Morgan, J. L., Heer, M., and Zwart, S. R. (2012) Space flight calcium: implications for astronaut health, spacecraft operations, and Earth. *Nutrients* **4,** 2047–2068
24. Massagli, T. L., and Cardenas, D. D. (1999) Immobilization hypercalcemia treatment with pamidronate disodium after spinal cord injury. *Arch. Phys. Med. Rehabil.* **80,** 998–1000
25. Kramer, I., Loots, G. G., Studer, A., Keller, H., and Kneissel, M. (2010) Parathyroid hormone (PTH)-induced bone gain is blunted in SOST overexpressing and deficient mice. *J. Bone Miner. Res.* **25,** 178–189
26. O'Brien, C. A., Plotkin, L. I., Galli, C., Goellner, J. J., Gortazar, A. R., Allen, M. R., Robling, A. G., Bouxsein, M., Schipani, E., Turner, C. H., Jilka, R. L., Weinstein, R. S., Manolagas, S. C., and Bellido, T. (2008) Control of bone mass and remodeling by PTH receptor signaling in osteocytes. *PLoS One* **3,** e2942
27. Costa, A. G., Cremers, S., Rubin, M. R., McMahon, D. J., Sliney, J., Jr., Lazaretti-Castro, M., Silverberg, S. J., and Bilezikian, J. P. (2011) Circulating sclerostin in disorders of parathyroid gland function. *J. Clin. Endocrinol. Metab.* **96,** 3804–3810
28. Yu, E. W., Kumbhani, R., Siwila-Sackman, E., and Leder, B. Z. (2011) Acute decline in serum sclerostin in response to PTH infusion in healthy men. *J. Clin. Endocrinol. Metab.* **96,** E1848–E1851
29. Bellido, T., Ali, A. A., Gubrij, I., Plotkin, L. I., Fu, Q., O'Brien, C. A., Manolagas, S. C., and Jilka, R. L. (2005) Chronic elevation of parathyroid hormone in mice reduces expression of sclerostin by osteocytes: a novel mechanism for hormonal control of osteoblastogenesis. *Endocrinology* **146,** 4577–4583
30. Powell, W. F., Jr., Barry, K. J., Tulum, I., Kobayashi, T., Harris, S. E., Bringhurst, F. R., and Pajevic, P. D. (2011) Targeted ablation of the PTH/PTHrP receptor in osteocytes impairs bone structure and homeostatic calcemic responses. *J. Endocrinol.* **209,** 21–32
31. Hughes, J. M., and Petit, M. A. (2010) Biological underpinnings of Frost's mechanostat thresholds: the important role of osteocytes. *J. Musculoskelet. Neuronal Interact.* **10,** 128–135
32. Bonewald, L. F. (1999) Establishment and characterization of an osteocyte-like cell line, MLO-Y4. *J. Bone Miner. Metab.* **17,** 61–65
33. Woo, S. M., Rosser, J., Dusevich, V., Kalajzic, I., and Bonewald, L. F. (2011) Cell line IDG-SW3 replicates osteoblast-to-late-osteocyte differentiation *in vitro* and accelerates bone formation *in vivo*. *J. Bone Miner. Res.* **26,** 2634–2646
34. Yu, L., van der Valk, M., Cao, J., Han, C. Y., Juan, T., Bass, M. B., Deshpande, C., Damore, M. A., Stanton, R., and Babij, P. (2011) Sclerostin expression is induced by BMPs in human Saos-2 osteosarcoma cells but not via direct effects on the sclerostin gene promoter or ECR5 element.

Bone **49,** 1131–1140
35. Fulzele, K., Krause, D. S., Panaroni, C., Saini, V., Barry, K. J., Liu, X., Lotinun, S., Baron, R., Bonewald, L., Feng, J. Q., Chen, M., Weinstein, L. S., Wu, J. Y., Kronenberg, H. M., Scadden, D. T., and Divieti Pajevic, P. (2013) Myelopoiesis is regulated by osteocytes through Gsα-dependent signaling. *Blood* **121,** 930–939
36. Wein, M. N., Spatz, J., Nishimori, S., Doench, J., Root, D., Babij, P., Nagano, K., Baron, R., Brooks, D., Bouxsein, M., Pajevic, P. D., and Kronenberg, H. M. (2015) HDAC5 controls MEF2C-driven sclerostin expression in osteocytes. *J. Bone Miner. Res.* **30,** 400–411
37. Kalajzic, I., Braut, A., Guo, D., Jiang, X., Kronenberg, M. S., Mina, M., Harris, M. A., Harris, S. E., and Rowe, D. W. (2004) Dentin matrix protein 1 expression during osteoblastic differentiation, generation of an osteocyte GFP-transgene. *Bone* **35,** 74–82
38. Hammond, T. G., and Hammond, J. M. (2001) Optimized suspension culture: the rotating-wall vessel. *Am. J. Physiol. Renal Physiol.* **281,** F12–F25
39. Papanicolaou, S. E., Phipps, R. J., Fyhrie, D. P., and Genetos, D. C. (2009) Modulation of sclerostin expression by mechanical loading and bone morphogenetic proteins in osteogenic cells. *Biorheology* **46,** 389–399
40. Li, J., Rose, E., Frances, D., Sun, Y., and You, L. (2012) Effect of oscillating fluid flow stimulation on osteocyte mRNA expression. *J. Biomech.* **45,** 247–251
41. Santos, A., Bakker, A. D., Zandieh-Doulabi, B., Semeins, C. M., and Klein-Nulend, J. (2009) Pulsating fluid flow modulates gene expression of proteins involved in Wnt signaling pathways in osteocytes. *J. Orthop. Res.* **27,** 1280–1287
42. Igwe, J. C., Gao, Q., Kizivat, T., Kao, W. W., and Kalajzic, I. (2011) Keratocan is expressed by osteoblasts and can modulate osteogenic differentiation. *Connect. Tissue Res.* **52,** 401–407
43. Paic, F., Igwe, J. C., Nori, R., Kronenberg, M. S., Franceschetti, T., Harrington, P., Kuo, L., Shin, D. G., Rowe, D. W., Harris, S. E., and Kalajzic, I. (2009) Identification of differentially expressed genes between osteoblasts and osteocytes. *Bone* **45,** 682–692
44. Bonnet, N., Standley, K. N., Bianchi, E. N., Stadelmann, V., Foti, M., Conway, S. J., and Ferrari, S. L. (2009) The matricellular protein periostin is required for SOST inhibition and the anabolic response to mechanical loading and physical activity. *J. Biol. Chem.* **284,** 35939–35950
45. Leupin, O., Kramer, I., Collette, N. M., Loots, G. G., Natt, F., Kneissel, M., and Keller, H. (2007) Control of the SOST bone enhancer by PTH using MEF2 transcription factors. *J. Bone Miner. Res.* **22,** 1957–1967
46. Wu, J. Y., Aarnisalo, P., Bastepe, M., Sinha, P., Fulzele, K., Selig, M. K., Chen, M., Poulton, I. J., Purton, L. E., Sims, N. A., Weinstein, L. S., and Kronenberg, H. M. (2011) Gsα enhances commitment of mesenchymal progenitors to the osteoblast lineage but restrains osteoblast differentiation in mice. *J. Clin. Investig.* **121,** 3492–3504
47. Loots, G. G., Keller, H., Leupin, O., Murugesh, D., Collette, N. M., and Genetos, D. C. (2012) TGF-β regulates sclerostin expression via the ECR5 enhancer. *Bone* **50,** 663–669
48. Nguyen, J., Tang, S. Y., Nguyen, D., and Alliston, T. (2013) Load regulates bone formation and Sclerostin expression through a TGFβ-dependent mechanism. *PLoS One* **8,** e53813
49. Capulli, M., Rufo, A., Teti, A., and Rucci, N. (2009) Global transcriptome analysis in mouse calvarial osteoblasts highlights sets of genes regulated by modeled microgravity and identifies a "mechanoresponsive osteoblast gene signature". *J. Cell. Biochem.* **107,** 240–252
50. Song, K., Wang, H., Zhang, B., Lim, M., Liu, Y., and Liu, T. (2013) Numerical simulation of fluid field and in vitro three-dimensional fabrication of tissue-engineered bones in a rotating bioreactor and *in vivo* implantation for repairing segmental bone defects. *Cell Stress Chaperones* **18,** 193–201
51. Jami, A., Gadi, J., Lee, M. J., Kim, E. J., Lee, M. J., Jung, H. S., Kim, H. H., and Lim, S. K. (2013) Pax6 expressed in osteocytes inhibits canonical Wnt signaling. *Mol. Cells* **35,** 305–312
52. Cherian, P. P., Cheng, B., Gu, S., Sprague, E., Bonewald, L. F., and Jiang, J. X. (2003) Effects of mechanical strain on the function of gap junctions in osteocytes are mediated through the prostaglandin EP2 receptor. *J. Biol. Chem.* **278,** 43146–43156
53. Zhang, K., Barragan-Adjemian, C., Ye, L., Kotha, S., Dallas, M., Lu, Y., Zhao, S., Harris, M., Harris, S. E., Feng, J. Q., and Bonewald, L. F. (2006) E11/gp38 selective expression in osteocytes: regulation by mechanical strain and role in dendrite elongation. *Mol. Cell. Biol.* **26,** 4539–4552
54. Galea, G. L., Sunters, A., Meakin, L. B., Zaman, G., Sugiyama, T., Lanyon, L. E., and Price, J. S. (2011) Sost down-regulation by mechanical strain in human osteoblastic cells involves PGE2 signaling via EP4. *FEBS Lett.* **585,** 2450–2454
55. Ito, T., Kurokouchi, K., Ohmori, S., Kanda, K., Murata, Y., Izumi, R., Iwata, H., and Seo, H. (1996) Changes in serum concentrations of calcium and its regulating hormones during tail suspension in rats. *Environ. Med.* **40,** 43–46
56. Genetos, D. C., Yellowley, C. E., and Loots, G. G. (2011) Prostaglandin E2 signals through PTGER2 to regulate sclerostin expression. *PLoS One* **6,** e17772
57. Hughes-Fulford, M. (2001) Changes in gene expression and signal transduction in microgravity. *J. Gravit. Physiol.* **8,** P1–P4
58. Cohen-Kfir, E., Artsi, H., Levin, A., Abramowitz, E., Bajayo, A., Gurt, I., Zhong, L., D'Urso, A., Toiber, D., Mostoslavsky, R., and Dresner-Pollak, R. (2011) Sirt1 is a regulator of bone mass and a repressor of Sost encoding for sclerostin, a bone formation inhibitor. *Endocrinology* **152,** 4514–4524
59. Yang, F., Tang, W., So, S., de Crombrugghe, B., and Zhang, C. (2010) Sclerostin is a direct target of osteoblast-specific transcription factor osterix. *Biochem. Biophys. Res. Commun.* **400,** 684–688
60. Bonnet, N., Conway, S. J., and Ferrari, S. L. (2012) Regulation of β catenin signaling and parathyroid hormone anabolic effects in bone by the matricellular protein periostin. *Proc. Natl. Acad. Sci. U.S.A.* **109,** 15048–15053
61. Macias, B. R., Aspenberg, P., and Agholme, F. (2013) Paradoxical Sost gene expression response to mechanical unloading in metaphyseal bone. *Bone* **53,** 515–519
62. Tu, X., Rhee, Y., Condon, K. W., Bivi, N., Allen, M. R., Dwyer, D., Stolina, M., Turner, C. H., Robling, A. G., Plotkin, L. I., and Bellido, T. (2012) Sost downregulation and local Wnt signaling are required for the osteogenic response to mechanical loading. *Bone* **50,** 209–217
63. Boukhechba, F., Balaguer, T., Michiels, J. F., Ackermann, K., Quincey, D., Bouler, J. M., Pyerin, W., Carle, G. F., and Rochet, N. (2009) Human primary osteocyte differentiation in a 3D culture system. *J. Bone Miner. Res.* **24,** 1927–1935
64. Honma, M., Ikebuchi, Y., Kariya, Y., and Suzuki, H. (2015) Establishment of optimized *in vitro* assay methods for evaluating osteocyte functions. *J. Bone Miner. Metab.* **33,** 73–84
65. Kenny, P. A., Lee, G. Y., Myers, C. A., Neve, R. M., Semeiks, J. R., Spellman, P. T., Lorenz, K., Lee, E. H., Barcellos-Hoff, M. H., Petersen, O. W., Gray, J. W., and Bissell, M. J. (2007) The morphologies of breast cancer cell lines in three-dimensional assays correlate with their profiles of gene expression. *Mol. Oncol.* **1,** 84–96
66. Zhu, J., Siclari, V. A., Liu, F., Spatz, J. M., Chandra, A., Divieti Pajevic, P., and Qin, L. (2012) Amphiregulin-EGFR signaling mediates the migration of bone marrow mesenchymal progenitors toward PTH-stimulated osteoblasts and osteocytes. *PLoS One* **7,** e50099
67. Arnold, M. A., Kim, Y., Czubryt, M. P., Phan, D., McAnally, J., Qi, X., Shelton, J. M., Richardson, J. A., Bassel-Duby, R., and Olson, E. N. (2007) MEF2C transcription factor controls chondrocyte hypertrophy and bone development. *Dev. Cell* **12,** 377–389
68. Sevetson, B., Taylor, S., and Pan, Y. (2004) Cbfa1/RUNX2 directs specific expression of the sclerosteosis gene (SOST). *J. Biol. Chem.* **279,** 13849–13858

The Wnt Inhibitor Sclerostin Is Up-regulated by Mechanical Unloading in Osteocytes *in Vitro*

Jordan M. Spatz, Marc N. Wein, Jonathan H. Gooi, Yili Qu, Jenna L. Garr, Shawn Liu, Kevin J. Barry, Yuhei Uda, Forest Lai, Christopher Dedic, Mercedes Balcells-Camps, Henry M. Kronenberg, Philip Babij and Paola Divieti Pajevic

J. Biol. Chem. 2015, 290:16744-16758.
doi: 10.1074/jbc.M114.628313 originally published online May 7, 2015